perature variation of many physical properties of a crystal, for example the mean-square displacement of the atoms from their equilibrium position in a crystal. Therefore, one proof of the worth of anharmonic parameters is the test whether they result in mean-square displacements which suit the experimental data well for the whole temperature range.

Further investigation on more extensive datasets therefore seems valuable and necessary.

References

ALBANESE, G., DERIU, A. & GHEZZI, C. (1976). *Acta Cryst.* A**32**, 904–909.

BARRON, T. H. K. & MUNN, R. W. (1967). *Acta Cryst.* **22**, 170–173.

FIELD, D. W. (1982). *Acta Cryst.* A**38**, 10–12.

HAMILTON, W. C. (1965). *Acta Cryst.* **18**, 502–510.

KURKI-SUONIO, K. (1977*a*). *Isr. J. Chem.* **16**(2, 3), 115–123.

KURKI-SUONIO, K. (1977*b*). *Isr. J. Chem.* **16**(2, 3), 132–136.

KURKI-SUONIO, K., MERISALO, M. & PELTONEN, H. (1979). *Phys. Scr.* **19**, 57–63.

MERISALO, M., JÄRVINEN, M. & KURITTU, J. (1978). *Phys. Scr.* **17**, 23–25.

MERISALO, M. & LARSEN, F. K. (1977). *Acta Cryst.* A**33**, 351–354.

MERISALO, M. & LARSEN, F. K. (1979). *Acta Cryst.* A**35**, 325–327.

MERISALO, M., PELJO, E. & SOININEN, J. (1978). *Phys. Lett. A*, **67**, 80–82.

PATHAK, P. D. & DESAI, R. J. (1981). *Phys. Status Solidi A*, **64**, 741–745.

ROSSMANITH, E. (1977). *Acta Cryst.* A**33**, 593–601.

ROSSMANITH, E. (1978). *Acta Cryst.* A**34**, 497–500.

ROSSMANITH, E. (1980). *Acta Cryst.* A**36**, 416–420.

SKELTON, E. F. & KATZ, J. L. (1968). *Phys. Rev.* **171**(3), 801–808.

VAHVASELKÄ, A. (1980). *Acta Cryst.* A**36**, 1050–1057.

Acta Cryst. (1984). B**40**, 249–256

Barium Diphosphate Tungsten Bronzes, $BaP_4O_8(WO_3)_{2m}$: X-ray Diffraction and High-Resolution Electron Microscopy Study

BY B. DOMENGÈS, M. HERVIEU AND B. RAVEAU

Laboratoire de Cristallographie, Chimie et Physique des Solides, LA 251, *ISMRA-Université*, 14032 *Caen CEDEX, France*

(*Received* 30 *May* 1983; *accepted* 3 *January* 1984)

Abstract

A new series of diphosphate tungsten bronzes (DPTB's), $BaP_4O_8(WO_3)_{2m}$, has been prepared and investigated by X-ray diffraction and electron microscopy. Five pure members, $6 \leq m \leq 10$, have been characterized; calculated electron microscope images simulate experimental images and confirm that they belong to the DPTB family whose structure is built up from ReO_3-type slabs connected through P_2O_7 groups. Electron diffraction showed that the Ba DPTB's exhibit remarkable differences with respect to the alkaline bronzes: existence of an *A*-type lattice, presence of superstructure reflections and stability. Many samples, with integer and non-integer *m* values ($m \leq 20$), have been studied in order to determine the homogeneity and the defects occurring in the Ba DPTB's: many crystals are characterized by disordered intergrowths; however, several ordered intergrowths of the $m = 8$ and $m = 9$ members have been observed. The behaviour and the stability of these bronzes are discussed and compared to those of the alkaline DPTB's.

Introduction

The recent investigation of the *A*–P–W–O system has shown the existence of a new series of bronzes, $A_xP_4O_8(WO_3)_{2m}$ with A = K, Rb, Tl (Giroult, Goreaud, Labbé & Raveau, 1980, 1981*a*, 1982, 1984; Labbé, Ouachee, Goreaud & Raveau, 1984; Hervieu & Raveau, 1982, 1983*a*, *b*). The host lattice of these compounds, called diphosphate tungsten bronzes (DPTB's), is built up from ReO_3-type slices connected through 'planes' of diphosphate groups forming hexagonal tunnels where the A^+ ions are located. For smaller ions such as Na^+ another tunnel structure is observed, $Na_xP_4O_8(WO_3)_{2m}$, called single phosphate tungsten bronzes (SPTB's) (Benmoussa, Groult, Labbé & Raveau, 1984); this latter structure is characterized by smaller but still hexagonal tunnels. This is to be compared to the A_xWO_3 bronzes of Magnéli (1949) which exhibit different tunnels according to the size of the A^+ ions. In this respect, the insertion of Ba^{2+} in such frameworks would be of interest since, in spite of its size being close to that of K^+, no Ba hexagonal tungsten bronze has been synthesized under atmospheric pressure; indeed, only tetragonal tungsten bronze Ba_xWO_3 ($0{\cdot}01 < x < 0{\cdot}33$) can be isolated (Conroy & Yokokawa, 1965; Ekström & Tilley, 1979). Moreover, the replacement of A^+ in these bronzes by Ba^{2+} could influence their electron-transport properties. Thus, the present work deals with the synthesis, X-ray diffraction and high-resolution electron microscopy (HREM) study of a new DPTB series, $BaP_4O_8(WO_3)_{2m}$.

0108-7681/84/030249-08$01.50

Experimental

Synthesis

Adequate mixtures of $BaCO_3$, $H(NH_4)_2PO_4$ and WO_3 (in the ratio $1/4/2m-1$) were first heated, at 873 K in air, in platinum crucibles in order to decompose the $BaCO_3$ and the $H(NH_4)_2PO_4$. The resulting products were then mixed with the necessary amount of metallic tungsten [1 mol per $(2m-1)$ WO_3] and heated in evacuated silica ampoules, at temperatures ranging from 1173 to 1473 K, for several days (6 to 21 d). The samples were then quenched to room temperature.

X-ray diffraction and electron microscopy analysis

All the samples were analysed by X-ray diffraction using a Guinier–de Wolff camera and the pure compounds were studied with a Philips powder diffractometer, using Cu $K\alpha$ radiation. The electron diffraction and electron microscopy observations were made with a JEOL 100CX transmission electron microscope operated at 120 kV. A multislice N-beam calculation of the two-dimensional lattice was performed with the program system developed by Skarnulis (1976). Through-focus series of images were calculated for different members. Parameters used in the calculations were: spherical-aberration constant $c_s = 0{\cdot}7$ mm, incident-beam convergence 0·1 mrad, defocus spread 170 Å, objective-aperture radius 0·42 $Å^{-1}$.

Integer-m members: $BaP_4O_8(WO_3)_{2m}$ $(6 \le m \le 10)$

The previous results obtained for the K and Rb DPTB's have shown that the experimental conditions (time and temperature) play an important role in their stabilization. Thus, different compositions corresponding to integer-m values, ranging from 2 to 20, have been synthesized using different temperatures and times and examined by X-ray and electron diffraction.

Among the different compositions, five pure oxides could be synthesized in the form of polycrystalline samples: $m=6$ (1373 K, 6 d); $m=7$ (1373 K, 9 d; 1473 K, 21 d); $m=8$ (1473 K, 10 d); $m=9$ (1293 K, 7 d); and $m=10$ (1373 K, 9 d). It must be pointed out that for $m \le 5$, we never observed an integer member of the series (by X-ray diffraction or by electron diffraction): indeed, for $m \le 3$ mixtures containing $P_8W_{12}O_{52}$ (Domengès, Goreaud, Labbé & Raveau, 1982) and, for $m=4$ and 5, mixtures of $P_4W_8O_{32}$ (Giroult *et al.*, 1981*b*, 1982), and tungsten suboxides or greater m-value members were observed. Moreover, it appears that the synthesis of the odd-m members is more difficult: so, for example, starting from a nominal composition for $m=9$, we obtained only a mixture of the two even-m members, $m=8$ and 10, after 9 d at 1253 K, but a mixture of $m=10$ and other phases was observed at a higher temperature (1373 K, 9 d). In a general manner, the stability of the Ba DPTB's seems to be lower than that of the K and Rb DPTB's.

Table 1. $BaP_4O_8(WO_3)_{2m}$: *crystallographic data*

m	a (Å)	b (Å)	c (Å)	β (°)
6	14·103 (3)	7·494 (1)	17·027 (5)	114·19 (2)
8	18·271 (4)	7·491 (2)	17·346 (4)	117·46 (2)
10	23·193 (4)	7·547 (2)	17·341 (2)	117·97 (1)
7	14·713 (3)	7·487 (2)	17·175 (7)	99·41 (3)

The parameters of the monoclinic cells deduced from the X-ray diffractograms (Table 1) are in agreement with the theoretical parameters obtained from the previously established equations (Hervieu & Raveau, 1982). However, the electron diffraction patterns brought out two differences with respect to the alkaline DPTB's. The first concerns the space groups of the Ba DPTB's: for whatever the m value, $6 \le m \le 10$, the extinction condition hkl, $h+l \neq 2n$ leads to the $A2/m$ group, in contrast to the alkaline DPTB's which exhibit two space groups according to the m values: $A2/m$ for $m=4$, 5 and 6 and $P2_1/c$ for $m=7$, 8, 9 and 10. The second point deals with the existence of superstructure reflections on the electron diffraction patterns, as already observed for alkaline DPTB's. However, the Ba DPTB's exhibit more complex phenomena as shown in Fig. 1. Such superstructure reflections are observed, for example, on the $h0l$ electron diffraction pattern of the $m=6$ member (Fig. 1*a*) where $h0l$ spots with odd-l values appear; a reciprocal-lattice study shows that they indicate a change of space group and, moreover, in these crystals, the intermediate sections of the reciprocal lattice often exhibit diffuse streaks. A more complex $h0l$ diagram is observed in Fig. 1(*b*) for an $m=7$ crystal; the superstructure reflections extend along $|\bar{2}02|^*$ and the measurement of the separation between pairs of spots indicates a superperiod of $5 \times d_{(\bar{2}02)}$ and $2 \times a$. The latter phenomenon may be due to a different stacking sequence of the P_2O_7 groups which connect the ReO_3-type slabs, involving a different distribution of the Ba^{2+} ions: however, the absence of modulation of the intensity of the spots did not allow a solution of this problem by HREM. Another type of superstructure reflections was observed on the $(hk0)$ plane of the member $m=10$ in Fig. 1(*c*); these involve a doubling of the 'a' parameter and the extinction condition hkl, $h+k \neq 2n$, for the superlattice cell. The weak superstructure reflections on the other sections of the reciprocal lattice did not allow a determination of the space group of the supercell. The reflections due to the basic structure of the latter type of crystal, which is rather rare, are characterized by a monoclinic cell different from the other crystals. This subcell indeed exhibits a β_{10} angle close to 92°, being different from $\beta_{10}=116°$, the angle generally observed for the other crystals. This difference between the two sorts

of crystals can be explained by a translation of one diphosphate plane out of two by $b/2$, as shown in Fig. 2. Thus it appears that, for $m = 10$, most of the crystals exhibit an 'a' axis parallel to the strings of octahedra, *i.e.* a type I cell with $(\beta_{10})_I \simeq 116°$ (Fig. 2a) whereas fewer crystals correspond to type II, *i.e.* to a cell with $(\beta_{10})_{II} \simeq 92°$. This phenomenon seems to be general for the even m members of this series since it has already been observed for the K and Rb bronzes: most of the crystals studied by electron diffraction exhibit a cell of the first type [$(\beta_m)_I$ close to 116°], whereas all the crystals of $m = 8$ and $m = 10$ which were studied by X-ray diffraction are of the second type [$(\beta_8)_{II} = 93{\cdot}89°$ and $(\beta_{10})_{II} = 91{\cdot}86°$]. An X-ray diffraction study of the type I crystals should be made in order to verify this hypothesis and to understand the arrangement of the octahedra which should be tilted in a different manner due to the translation of the P_2O_7 groups. Moreover the Ba DPTB's may bring more information owing to the high atomic number of Ba, if one assumes that the positions of the A^+ ions are closely related to that of the diphosphate groups as previously proposed (Giroult *et al.*, 1982).

The HREM study confirms the structure of these bronzes. Figs. 3 and 4 show as examples the HREM micrographs of the members $m = 6$ and $m = 7$. The distribution of the white spots, and their distances, suggest that they correspond to the tunnels of the structure; the white spots (H) located along the darker rows are attributed to the hexagonal tunnels, whereas the white spots (P) between these rows would correspond to the perovskite tunnels, as can be seen from a comparison of Figs. 3(a) and 3(b), and Figs. 4(a) and 4(b) respectively. The contrasts are in agreement

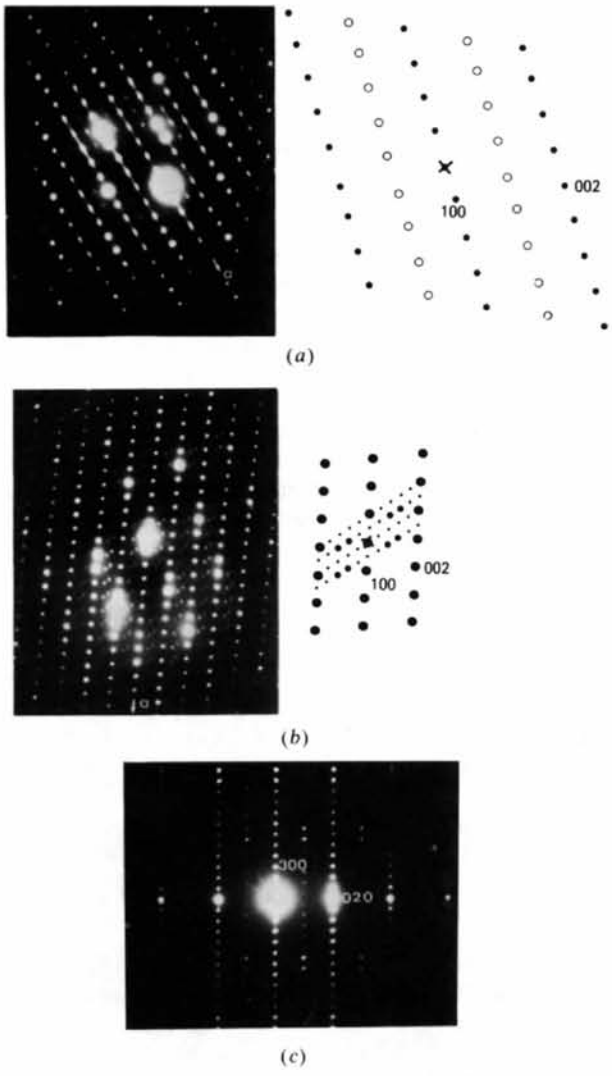

Fig. 1. (010) electron diffraction patterns of $BaP_4O_8(WO_3)_{2m}$ members: (a) $m = 6$, (b) $m = 7$ and their idealized drawings; (c) $m = 10$.

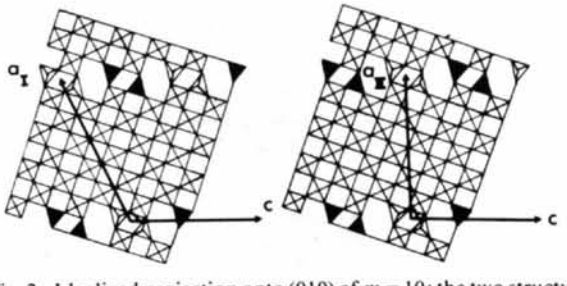

Fig. 2. Idealized projection onto (010) of $m = 10$; the two structures differ by a translation of one diphosphate plane out of two by $b/2$. (a) $(\beta_{10})_I$ 116°; (b) $(\beta_{10})_{II}$ 92°.

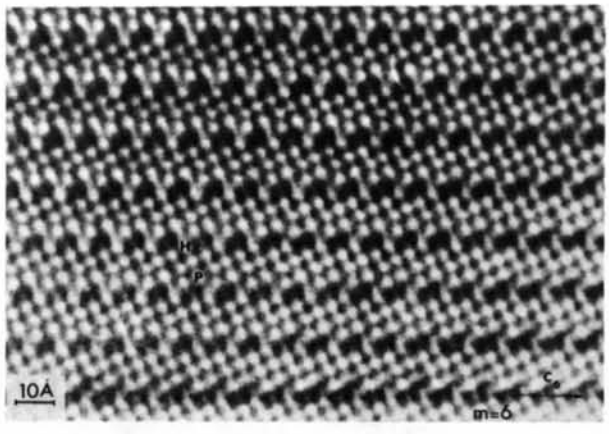

Fig. 3. (a) An image of $BaP_4O_8(WO_3)_{12}$ projected down [010] at about −600 Å underfocus. The white spots are perovskite (P) and hexagonal (H) tunnels. (b) Idealized structure of $m = 6$.

with the structure in spite of the partial occupancy of the hexagonal tunnels by the Ba^{2+} ions. In order to confirm this hypothesis, images were simulated using the programs *F. COEFF* and *F. DEFECT* (Skarnulis, 1976). Starting from the models deduced from the X-ray diffraction results for $Rb_xP_4O_8(WO_3)_{2m}$ bronzes (Giroult *et al.*, 1980, 1981*a*, 1982), calculations were made with different conditions of focus (underfocus of 0 to 1400 Å) and different crystal thicknesses (from 19 to 76 Å). Figs. 5 and 6 show some of the resulting calculated images for $m = 6$ and $m = 7$ respectively (for crystal thicknesses 22, and 19 Å respectively); the images oscillate rapidly with defocus Δf. The images calculated at optimum defocus (−600 Å) show a direct representation of the projection of the structure in the incident-beam direction. Similar results were obtained for the other integer members of the series, as shown for example for $m = 8$ and $m = 9$ (Fig. 7).

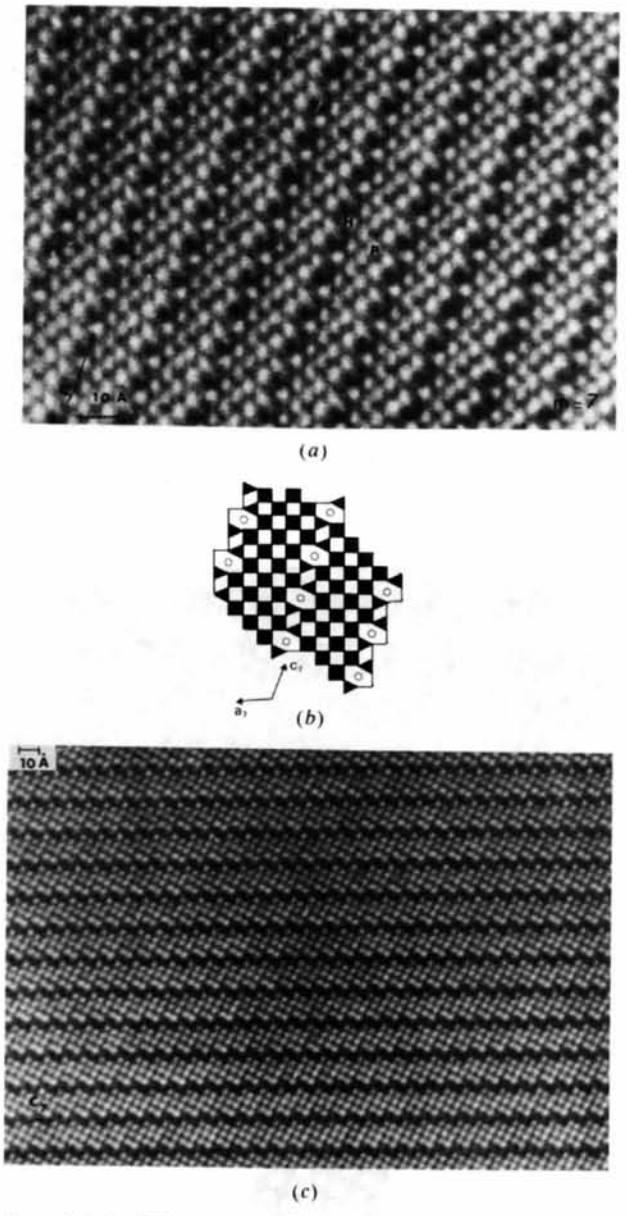

Fig. 4. (*a*) Enlargement of an electron micrograph of $BaP_4O_8(WO_3)_{14}$. The image was taken at about −600 Å underfocus. White (*H*) and (*P*) spots represent the tunnels of the structure. (*b*) Idealized structure of $m = 7$. (*c*) The same image for $\Delta f = -800$ Å.

Non-stoichiometry and defects

Superior integer-m members, $m > 10$

For $m > 10$, no integer-m member could be isolated in the form of a pure phase. The X-ray diffraction patterns always showed the formation of a mixture of microphases. The electron diffraction study of these phases allowed us to observe three sorts of crystals:

– perfectly ordered microcrystals, corresponding to the integer-m members, $m = 11$, 12, 13, 14, 15, 16 and 17. Fig. 8 shows a micrograph of such a crystal corresponding to a regular sequence of $m = 15$. It

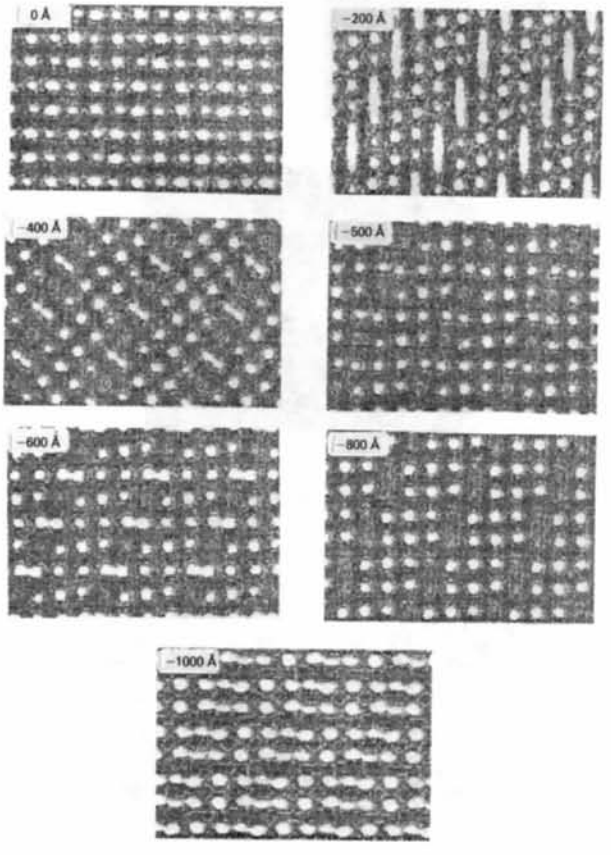

Fig. 5. Calculated through-focus images of the $BaP_4O_8(WO_3)_{12}$ structure ($\Delta f = 0$, −200, −400, −500, −600, −800 and −1000 Å).

should be noted that the m values observed in a microcrystal are always smaller than the nominal composition m as shown by the histogram for a sample of $m = 20$ (Fig. 9).

– very disordered microcrystals (characterized by a change in stacking sequences) whose electron diffraction patterns show diffuse streaks along $\mathbf{a}^*$, for which the m value cannot be identified.

– tungsten suboxides, W_nO_{3n-1} and W_nO_{3n-2}, with many defects.

Besides the disorder phenomena, these crystals exhibit defects similar to those observed in the K and Rb DPTB's (Hervieu & Raveau, 1983*a*), *i.e.* stopping of the rows of P_2O_7 groups leading to large ReO_3-type domains breaking and translation of the P_2O_7 rows. This latter defect, which has been interpreted previously, is shown on the micrograph of a crystal of nominal composition $m = 20$ (Fig. 10).

Non-integer-m member ($m < 10$) *and disordered integer members*

For non-integer-m compositions, no pure phase could be isolated in the form of polycrystalline samples in signficant amounts. However, many crys-

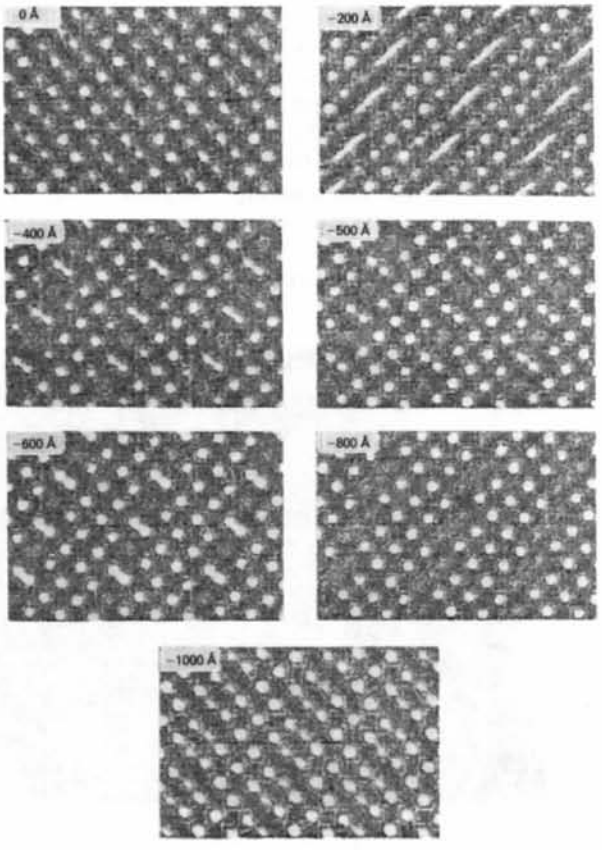

Fig. 6. Calculated through-focus images of $BaP_4O_8(WO_3)_{14}$ (Δf = 0, −200, −400, −500, −600, −800, −1000 Å).

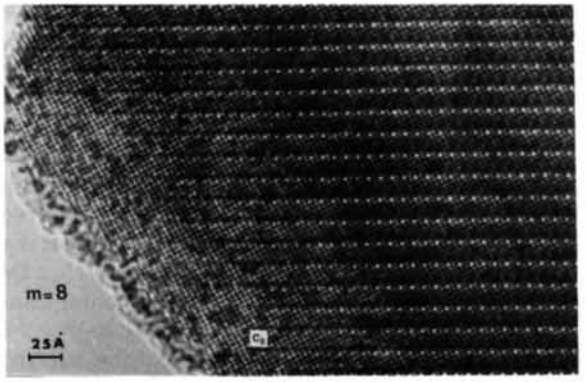

(*a*)

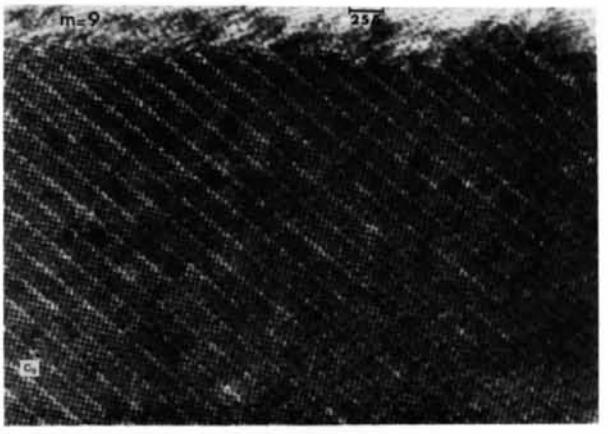

(*b*)

Fig. 7. High-resolution micrograph of integer-m members. (*a*) $m = 8$ ($\Delta f = -600$ Å); (*b*) $m = 9$ ($\Delta f = -500$ Å).

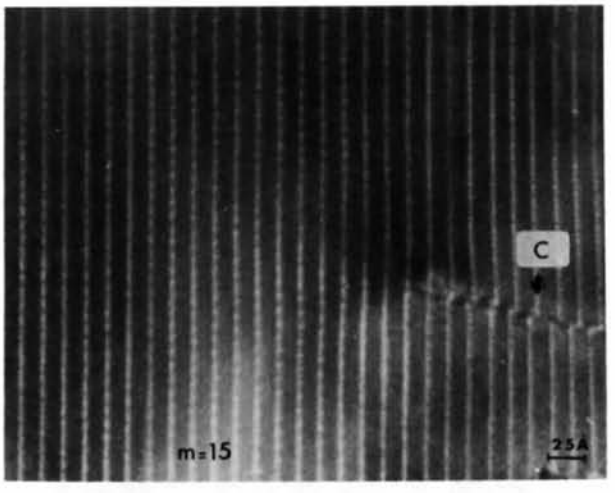

Fig. 8. Electron micrograph of a regular member $m = 15$. The crystal shows evidence (black arrow) of a '*C*' defect (Hervieu & Raveau, 1983*a*) corresponding to the breaking of pyrophosphate planes.

tals observed by electron microscopy exhibit an intergrowth of integer-m members. Most of them were characterized by disordered intergrowths; this was also observed for crystals of nominal composition $m=9$, as shown for the $h0l$ micrograph (Fig. 11) which corresponds to a disordered sequence of the members $m=8$, 9 and 10. It is worth noting that the disordered intergrowth is often observed for the nominal composition $m=9$, in agreement with the X-ray diffracton results which indicate that this member is difficult to synthesize as a pure compound. For nominal compositions corresponding to $m=9$ or close to this value, several crystals exhibit electron diffraction patterns with superstructure reflections along **a*** which correspond to the superposition of two sets of reflections. The electron microscopy study of these crystals has shown that these phenomena correspond to an ordered intergrowth of two members having each large domains. The HREM micrograph of Fig. 12 shows the ordered intergrowth |8:9| which corresponds to the regular sequence of the members

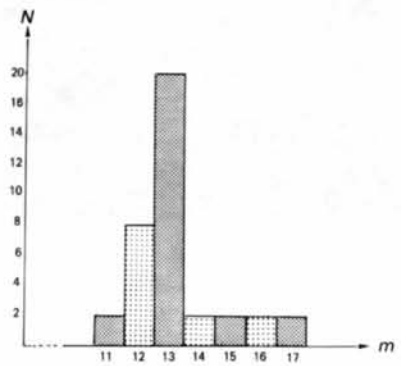

Fig. 9. The distribution of the m values obtained from the electron diffraction of 38 different crystal fragments.

$m=8$ and $m=9$. For the same nominal composition, more complex ordered intergrowths were observed, as shown from the low-resolution micrograph (Fig. 13) which corresponds to the sequence |8:8:9:9|.

Some of the disordered crystals are twinned as shown in Fig. 14 for a crystal of nominal composition $m=9$. This micrograph (Fig. 14*a*) shows that the two domains, I and II, are identical and correspond to a disordered intergrowth of the members $m=8$, 9 and 10. The diffraction patterns and the HREM micrographs show that the corresponding (010) planes are slightly tilted with respect to each other and that the C_I and C_{II} axes make an angle of 113°. The high-resolution micrograph (Fig. 14) of a very thin area shows that the boundary is oriented along $|201|^{I}_{ReO_3}$ with respect to the first domain and along $|001|^{II}_{ReO_3}$ with respect to the second; the domain boundary exhibits a variable width (up to 70 Å). This twin wall therefore involves a disturbed zone of finite thickness between the two lattices. It is difficult to give an exact interpretation of this phenomenon because of the coexistence of different members ($m=8$, 9 and 10) in a disordered state. Nevertheless, the formation of pentagonal tunnels would correctly explain this junction as shown in Fig. 14(*c*); this model of the junction between two domains of $m=9$ and $m=10$ members indeed exhibits an angle of 113° between C_I and C_{II}, very close to the observed value.

It should be pointed out that for Ba as well as for K and Rb, 'twinned' domains similar to those observed for crystallographic shear (CS) structures (Sundberg & Tilley, 1974*a*; Iijima, 1975; Sahle & Sundberg, 1980; Tilley, 1978) were not observed in spite of the close relationship between these two families. This may be due to the presence of diphosphate groups which would impose a different distortion of the octahedral framework.

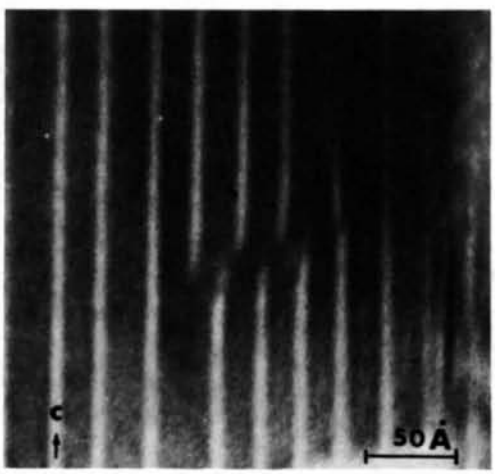

Fig. 10. Low-resolution image of a '*C*' defect corresponding to the breaking and the translation of diphosphate planes in a crystal fragment of nominal composition $m=20$.

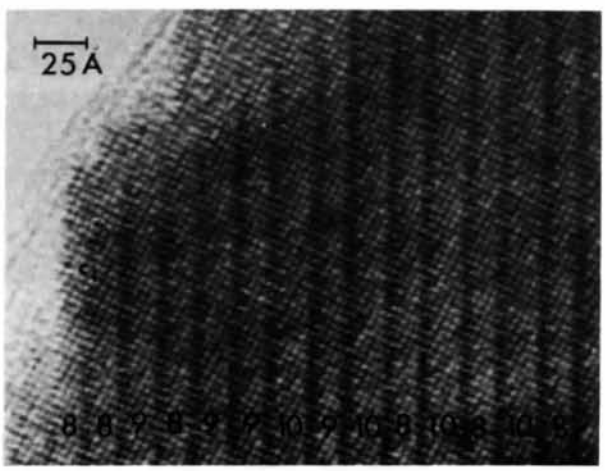

Fig. 11. Electron micrograph of a disordered crystal of nominal composition $m=9$ corresponding to the intergrowth of $m=8$, 9 and 10 members.

Conclusion

A new series of DPTB's $BaP_4O_8(WO_3)_{2m}$, has been obtained. These bronzes behave differently from hexagonal tungsten bronzes (HTB's): Ba DPTB's can indeed be synthesized whereas no Ba HTB's have been prepared under normal conditions.

In spite of their structural similarity to the other DPTB's the Ba DPTB's exhibit some important differences. Unlike the alkaline bronzes the Ba bronzes are always characterized by an *A*-type lattice whatever the *m* value may be, and a rather large number of crystals show superstructure reflections. These differences may be due to the highly covalent nature of Ba which may form Ba–O σ-type bonds with the O atoms of the framework. They could correspond to possible translations of the P_2O_7 groups along **b**, involving order–disorder phenomena in the distribution of the Ba^{2+} ions in the tunnels and different ways of tilting the WO_6 octahedra. In this respect, the X-ray diffraction study of Ba even-*m*-member crystals characterized by a '116° monoclinic cell' will certainly be important in order to understand these phenomena. The influence of the Ba stoichiometry, which brings twice as many electrons to the framework as the univalent ions, should also be considered.

The Ba DPTB's also differ from the alkaline DPTB's by their stability. It is indeed noteworthy that

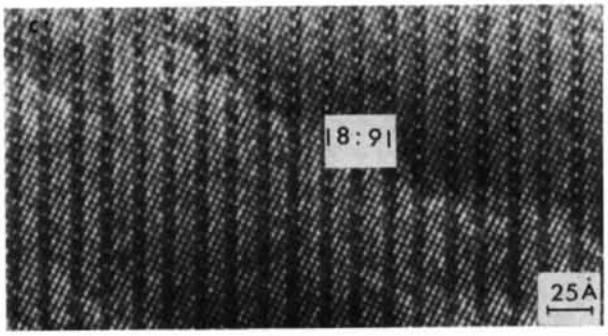

(*a*)

(*b*)

Fig. 12. (*a*) Ordered intergrowth |8:9| observed in an $m = 9$ crystal and (*b*) its electron diffraction pattern.

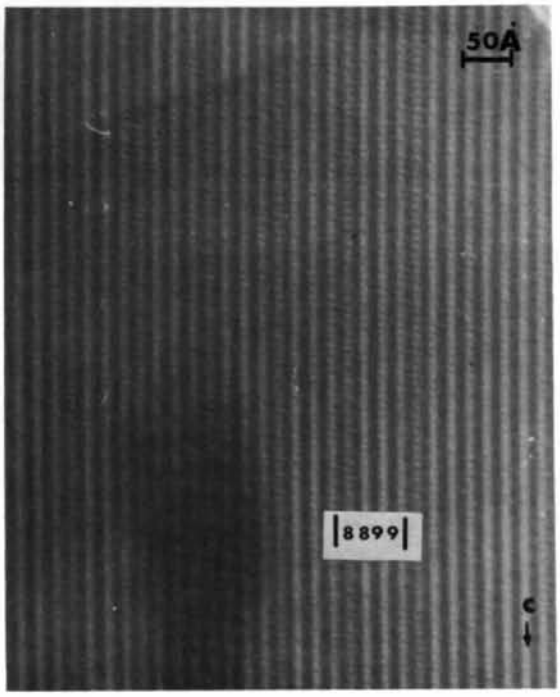

(*a*)

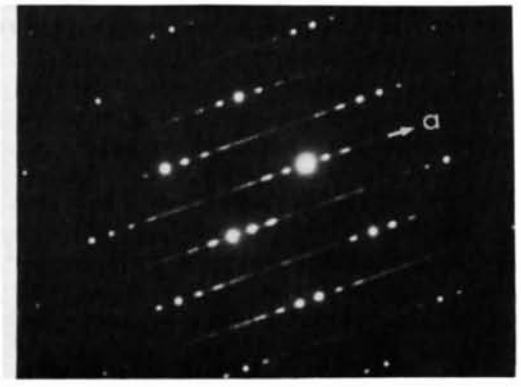

(*b*)

Fig. 13. (*a*) Low-resolution image of an |8:8:9:9| intergrowth observed in a crystal fragment of nominal composition $m = 9$ and (*b*) its electron diffraction pattern.

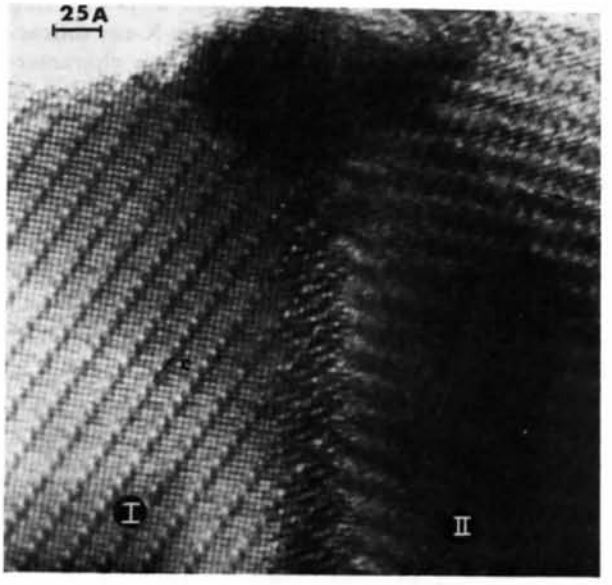

(*a*)

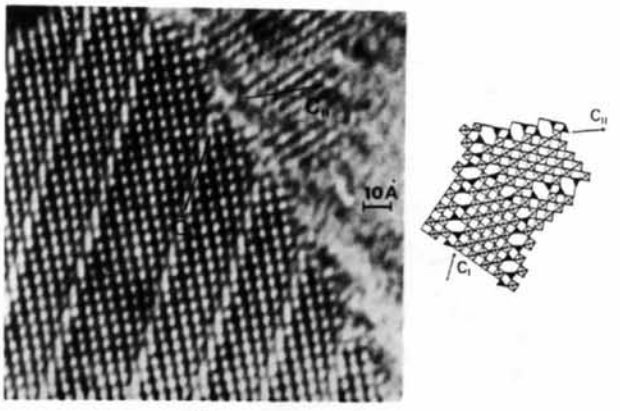

(*b*)

Fig. 14. (*a*) $m=9$: electron micrograph of a crystal exhibiting orientated domains (denoted I and II). (*b*) Enlargement of a thin edge and (*c*) hypothesis of junction between the two domains. In the two micrographs, domain II is misaligned owing to the small tilt between the domains.

a smaller number of integral members could be synthesized as pure phases in the case of Ba. On the other hand, it is also remarkable that these bronzes do not exhibit CS defects, unlike the K and Rb DPTB's in which CS planes could be formed during the synthesis or in the electron microscope during observations (Sundberg & Tilley, 1974*b*; Sundberg, 1980). This difference is also important for the study of the electron-transport properties of the DPTB family, since the presence of CS defects may modify these properties. The possibility of intergrowth of the CS structures and Ba DPTB's will be investigated.

References

BENMOUSSA, A., GROULT, B., LABBÉ, PH. & RAVEAU, B. (1984). *Acta Cryst.* C**40**, 573–576.

CONROY, L. E. & YOKOKAWA, T. (1965). *Inorg. Chem.* **4**, 994–996.

DOMENGÈS, B., GOREAUD, M., LABBÉ, PH. & RAVEAU, B. (1982). *Acta Cryst.* B**38**, 1724–1728.

EKSTRÖM, T. & TILLEY, R. J. D. (1979). *J. Solid State Chem.* **28**, 259–268.

GIROULT, J. P., GOREAUD, M., LABBÉ, PH. & RAVEAU, B. (1980). *Acta Cryst.* B**36**, 2570–2575.

GIROULT, J. P., GOREAUD, M., LABBÉ, PH. & RAVEAU, B. (1981*a*). *Acta Cryst.* B**37**, 1163–1166.

GIROULT, J. P., GOREAUD, M., LABBÉ, PH. & RAVEAU, B. (1981*b*). *Acta Cryst.* B**37**, 2139–2142.

GIROULT, J. P., GOREAUD, M., LABBÉ, PH. & RAVEAU, B. (1982). *Acta Cryst.* B**38**, 2342–2347.

GIROULT, J. P., GOREAUD, M., LABBÉ, PH. & RAVEAU, B. (1984). *Rev. Chim. Minér.* To be published.

HERVIEU, M. & RAVEAU, B. (1982). *J. Solid State Chem.* **43**, 299–308.

HERVIEU, M. & RAVEAU, B. (1983*a*). *Chem. Scr.* **22**, 117.

HERVIEU, M. & RAVEAU, B. (1983*b*). *Chem. Scr.* **22**, 123.

IIJIMA, S. (1975). *J. Solid State Chem.* **14**, 52–65.

LABBÉ, PH., OUACHEE, D., GOREAUD, M. & RAVEAU, B. (1984). *J. Solid State Chem.* To be published.

MAGNÉLI, A. (1949). *Ark. Kemi*, **1**, 213–221.

SAHLE, W. & SUNDBERG, M. (1980). *Chem. Scr.* **16**, 163–168.

SKARNULIS, A. J. (1976). Thesis. Arizona State Univ.

SUNDBERG, M. (1980). *J. Solid State Chem.* **35**, 120–127.

SUNDBERG, M. & TILLEY, R. J. D. (1974*a*). *J. Solid State Chem.* **11**, 150–160.

SUNDBERG, M. & TILLEY, R. J. D. (1974*b*). *Phys. Status Solidi A*, **22**, 677–684.

TILLEY, R. J. D. (1978). *Chem. Scr.* **14**, 147–159.